Local Sampling of the Wigner Function at Telecom Wavelength with Loss-Tolerant Detection of Photon Statistics

G. Harder,[1] Ch. Silberhorn,[1,2] J. Rehacek,[3] Z. Hradil,[3] L. Motka,[3] B. Stoklasa,[3] and L. L. Sánchez-Soto[4,2]
[1]Department of Physics, University of Paderborn, Warburger Straße 100, 33098 Paderborn, Germany
[2]Max-Planck-Institut für die Physik des Lichts, Günther-Scharowsky-Straße 1, Bau 24, 91058 Erlangen, Germany
[3]Department of Optics, Palacký University, 17. listopadu 12, 77146 Olomouc, Czech Republic
[4]Departamento de Óptica, Facultad de Física, Universidad Complutense, 28040 Madrid, Spain
(Received 11 January 2016; published 30 March 2016)

We report the experimental point-by-point sampling of the Wigner function for nonclassical states created in an ultrafast pulsed type-II parametric down-conversion source. We use a loss-tolerant time-multiplexed detector based on a fiber-optical setup and a pair of photon-number-resolving avalanche photodiodes. By capitalizing on an expedient data-pattern tomography, we assess the properties of the light states with outstanding accuracy. The method allows us to reliably infer the squeezing of genuine two-mode states without any phase reference.

DOI: 10.1103/PhysRevLett.116.133601

Modern quantum technologies hinge on the capability to generate, manipulate, and measure quantum states. A successful experimental procedure requires verification of each of these steps: this is the scope of quantum tomography [1].

Light is of particular significance in most of those developments because it is unique as an information carrier. In quantum optics, the continuous-variable community is mostly concerned with the wave aspects of light, looking chiefly at quantities such as quantum noise, squeezing, and entanglement. Homodyne detection is then the technique of choice since it allows for a direct reconstruction of the Wigner function in terms of the field quadratures [2].

Interestingly enough, the Wigner function can also be determined at a single point in phase space by measuring the parity [3]. The complete function can then be sampled if this measurement is performed at a sufficient number of points. This direct probing was first demonstrated with motional states of a trapped ion [4] and applied with great success to Fock states in cavity quantum electrodynamics [5].

In optics, this method can be implemented with a highly asymmetric beam splitter, which superimposes the quantum signal of interest with a coherent reference field (which occasionally can be as weak as the signal [6,7]), followed by photon counting [8,9]. Despite its simplicity, the approach places stringent demands on detector performance and requires a full photon-number resolving (PNR) capability [10–14], which, in fact, limits its practical applicability. The same complication arises in other alternative methods [15].

A promising PNR detection strategy has recently been demonstrated [16–18]. It is based on time-multiplexed detection (TMD) with avalanche photodiodes (APDs) and works even with pulses [19]. For visible light, this has been used to implement a first direct probing for heralded single photons [20]. However, at the telecom wavelengths employed in our experiment, the established technology is based on InGaAs APDs, which are plagued by high dark-count rates and long dead times, thereby making gating essential.

The effective implementation of these advanced schemes thus demands an accurate knowledge of the detector [21–27]. To address this issue, we adopt here the so-called fitting of data patterns, an approach proposed in Refs. [28,29] and experimentally realized in several groups [30–32]. This technique enables calibration of detectors with a sizable number of outcomes and their subsequent use in state estimation. It does not extract the complete set of operators that describe the detector, but rather uses the raw measurement outcome distributions for known input states as the detector calibration. Besides, there is no need for any numerical postprocessing. In this Letter we use the pattern tomography as an efficient tool to probe point by point the Wigner function of pulsed single photons and two-mode squeezed states at telecom wavelengths. Thereby, we achieve the inference of mode-selective, genuine two-mode squeezing without phase reference.

For a single-mode field, represented by the density operator $\hat{\rho}$, the direct probing is based on the observation that the Wigner function at the point α of the phase space can be expressed as the average value of the parity operator on the probed quantum state $\hat{\rho}$ displaced by $-\alpha$ [8,9]: viz.,

$$W(\alpha) = \frac{2}{\pi}\mathrm{Tr}[\hat{D}^{\dagger}(\alpha)\hat{\rho}\,\hat{D}(\alpha)\hat{\Pi}] = \frac{2}{\pi}\sum_{n}(-1)^{n}\rho_{nn}(-\alpha). \quad (1)$$

Here, $\hat{\Pi}=\exp(i\pi\hat{a}^{\dagger}\hat{a})$ is the parity, whose eigenstates are the Fock states $|n\rangle$, with eigenvalues $(-1)^n$, $\hat{a}$ and $\hat{a}^{\dagger}$ are photon annihilation and creation operators, $\hat{\rho}(-\alpha)=\hat{D}^{\dagger}(\alpha)\hat{\rho}\hat{D}(\alpha)$, and $\hat{D}(\alpha)=\exp(\alpha\hat{a}^{\dagger}-\alpha^{*}\hat{a})$ is the displacement.

There are significant differences between this direct probing and homodyne tomography. The latter is a Gaussian measurement that projects the state along a field quadrature. A PNR detector, on the other hand, projects onto the photon-number basis, which is a non-Gaussian operation.

Another important distinction is the fact that homodyne detection involves an intrinsic filtering: only the part of the signal that overlaps with the local oscillator can be seen by the detector. Losses and mode mismatch yield the same signature.

Conversely, direct probing detects all the modes, which results in a more complete characterization with an intrinsic quantification of the mode overlap. For a nonunity overlap $\mathcal{M}$ with the reference beam, the measured Wigner function is the product of the state and vacuum Wigner functions: $W(\alpha) = W_{\text{state}}(\sqrt{\mathcal{M}}\alpha)W_{\text{vac}}(\sqrt{1-\mathcal{M}}\alpha)$. This behavior is fundamentally different from losses and is crucial to estimating both the losses and the overlap with the local oscillator.

To sum up, homodyne detection is mode selective and insensitive to detrimental effects from other modes and backgrounds. Direct probing is sensitive to all modes and to the spatial-spectral single-mode characteristics of the states.

To demonstrate the capabilities of the direct probing, we choose a pulsed single-photon state with a single-mode spectral structure, i.e., with a diagonal density matrix. This simplifies the detection scheme, preventing the need for phase sensitivity. Consequently, we use parametric down-conversion (PDC), a nonlinear process in which one pump photon decays into two twin photons, called the signal and the idler. Ideally, the output of a PDC source is the two-mode squeezed vacuum

$$|\Psi\rangle = \sqrt{1-\lambda^2}\sum_n \lambda^n |n,n\rangle, \tag{2}$$

where n is the photon number in each mode, $\lambda = \tanh(r)$, and r is the squeezing parameter, which scales linearly with the pump field amplitude, the nonlinear coefficient $\chi^{(2)}$ of the medium, and the interaction length inside the crystal.

In the absence of losses, the perfect photon-number correlations of this state allow for heralding Fock states in one mode by conditioning on certain photon numbers in the other. With losses, the heralded states can still look pretty much like Fock states and can show nonclassical statistics.

These correlations can be clearly appreciated using the Wigner function of the PDC state (2), which is

$$W(\alpha,\beta) = \frac{4}{\pi^2}\exp\left(-e^{2r}|\alpha+\beta^* e^{-i\phi}|^2 - e^{-2r}|\alpha-\beta^* e^{-i\phi}|^2\right), \tag{3}$$

where α and β are the complex quadratures of the modes and ϕ comes from the phase of the pump. For infinite squeezing $r \to \infty$, we have $|\alpha+\beta^* e^{-i\phi}| = 0$; i.e., the positions (real parts α_r and β_r) and the momenta (imaginary parts α_i and β_i) are perfectly correlated or anticorrelated, as indicated by the arrows in Fig. 1(a). For a finite r, the variance of the correlations is $\text{Var}(|\alpha+\beta^* e^{-i\phi}|) = e^{-2r}$, which is below the Heisenberg limit of coherent states by a factor of e^{-2r}, a signature of entanglement between the two modes. Such correlations could be measured in a balanced homodyne setup, but it is experimentally challenging, as pump and local oscillator phases have to be locked.

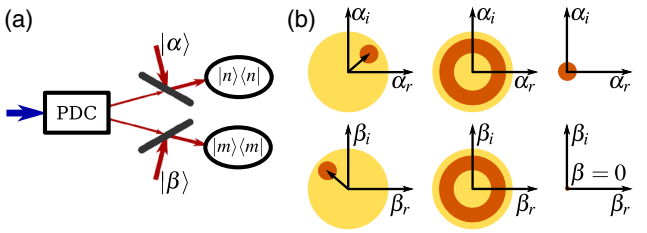

FIG. 1. Phase-space correlations in PDC. (a) Direct probing scheme with two displacement beams, α and β, and PNR measurements. The marginal distributions of signal or idler are indicated by the larger circles, while correlations are indicated by the darker circles. (b) Phase-averaged state, where only the amplitudes remain correlated. Specifically, the distribution for $\beta = 0$ shows correlations below the corresponding ones for the vacuum, from which the initial squeezing can be inferred.

Since we cannot access this phase, this is tantamount to averaging over it, which yields the state

$$W_{\text{avg}}(\alpha,\beta) = \frac{4}{\pi^2}\exp[-2\cosh(2r)(|\alpha|^2+|\beta|^2)] \times I_0(-4\sinh(2r)|\alpha||\beta|), \tag{4}$$

where $I_0(x)$ is the modified Bessel function. This W_{avg} depends only on the amplitudes $|\alpha|$ and $|\beta|$. Correspondingly, one can only measure photon numbers and obtain information about the diagonal elements of the density matrix. The off-diagonal elements remain hidden and entanglement is lost.

Nonetheless, the correlations are still present around the origin, as sketched in Fig. 1(b): if we set $\beta = 0$, the distribution of $|\alpha|$ is narrower by a factor of $\cosh(2r)$ than the corresponding one for the vacuum, which can be verified with direct probing.

Our experimental setup is schematized in Fig. 2. We use PDC in an 8 mm long periodically poled potassium titanyl phosphate waveguide. The process is pumped with 0.5 ps pulses at a wavelength of 768 nm, producing orthogonally polarized signal and idler beams at 1536 nm. The signal and idler modes are decorrelated in frequency, enabling the heralding of nearly pure states [33].

We overlap the signal with a coherent reference beam in an asymmetric beam splitter with a 90:10 splitting ratio, consisting of a half-wave plate and a polarizing beam splitter. In the limit of unity transmission and perfect mode overlap, this corresponds to the displacement operator $\hat{D}(\alpha)$ [8]. To maximize the mode overlap, the reference beam has to match the signal mode, both spectrally and temporally. Therefore, we perform spectral shaping with a $4f$ spectrometer made of two gratings and two lenses, all separated by the focal length of the lenses. In the Fourier plane of this spectrometer, we use a variable slit which can be rotated around the propagation axis; this allows us to shape the reference spectrum to a Gaussian form matching the spectrum of the PDC mode. The temporal overlap is achieved with a translation stage in the reference beam. From Hong-Ou-Mandel dips between the reference and the signal, we estimate the overlap $\mathcal{M}$ to be around 0.7.

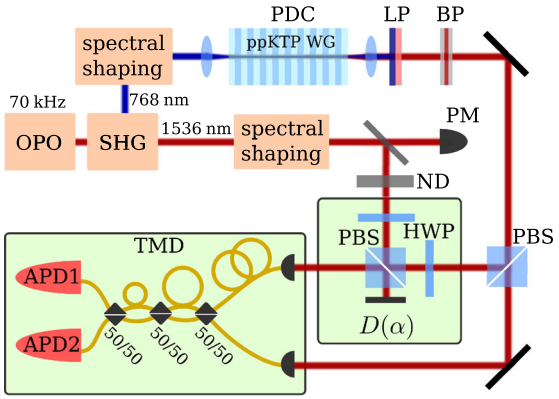

FIG. 2. Experimental setup. Pulsed light from an optical parametric oscillator (OPO) is frequency doubled by second harmonic generation (SHG) and spectrally shaped in a $4f$ line. After the PDC, the pump is filtered with a long pass filter (LP) and the sinc sidelobes of the PDC spectrum and unwanted background are suppressed with a bandpass filter (BF). Signal and idler are split at a polarizing beam splitter (PBS). The reference beam, monitored with a power meter (PM), is filtered to the single-photon level using neutral density filters (NDs) and overlapped with the idler at a 90:10 coupler consisting of a half-wave plate (HWP) and a PBS. This realizes the displacement operation $\hat{D}(\alpha)$. Both states are coupled into single-mode fibers and measured with an eight-bin, two-mode TMD.

Both output ports are measured with a TMD. One mode is delayed at the input of the TMD and then each mode is split into four temporal bins and two spacial bins at 50:50 beam splitters. In total, this amounts to 16 bins such that up to eight photons per mode can be measured. Each pulse impinges onto one of two InGaAs APDs with detection efficiencies around 20%. InGaAs APDs have the detrimental effect of afterpulsing, which means that after a detection there is a finite probability (~7%) of a subsequent detection without a photon being present. This makes the analysis of TMD data extremely difficult, as afterpulses modify the photon-number distribution in a nontrivial way.

Some detector tomography is therefore necessary to reliably extract the photon statistics of the incoming modes. Fitting of data patterns is ideally suited for this task (see the Supplemental Material for details [34]). It requires knowledge of the detector outputs for certified input probes. We use coherent states already present as the reference beam and couple them into both inputs of the TMD with different power settings adjusted by motorized half-wave plates and polarizing beam splitters.

Powers are calibrated with respect to the power at the input fiber of the TMD. Hence, losses inside the TMD and quantum efficiency of the APDs are accounted for by the tomography. Losses inside the waveguide, subsequent optical elements, and the fiber incoupling must be included in the reconstructed state. This is the most meaningful separation between the generation and the detection parts, as it is the point at which the source would be combined with other sources or integrated into a larger network.

The displaced PDC states are measured with the TMD. The joint photon-number distribution P_{mn} of each displaced state is estimated using pattern tomography and the corresponding parity $S(|\alpha|) = \sum_{mn}(-1)^{m+n}P_{mn}(|\alpha|)$ calculated, where $P_{mn}(|\alpha|)$ is the reconstructed two-mode photon-number distribution with signal mode displaced by $|\alpha|$. The measured parity values can be immediately converted to a Wigner function: $W(|\alpha|) = 4S(|\alpha|)/\pi^2$.

Pattern tomography makes use of a set of 639 two-mode coherent probes with known signal or idler amplitudes in the range $0 < |\alpha(\xi)| < 3.5$. The probes are measured with the TMD and the corresponding patterns are recorded. A sample of 100 patterns is used for any single reconstruction, as this matches well a typical number of linearly independent TMD outcomes for moderately intense signals. The reconstruction is repeated with different randomly chosen samples of pattern subsets. This makes it possible to estimate the errors and calculate the final reconstruction averaging over pattern sampling.

To compare the experimentally obtained parities with the theoretical predictions, one has to know the reference displacements, as well as the squeezing r and the coupling efficiency η. Displacements are determined by measuring the reference beam alone and comparing the probabilities of zero detection with those of the coherent probes. A least-squares fit is sufficient for this purpose. Additionally, the original undisplaced PDC state is measured to estimate the squeezing parameter $r \approx 0.6$ and coupling efficiency $\eta \approx 0.75$: these are the values for which the theory provides the best fit.

Figure 3 shows the parity of the displaced PDC state, as estimated from the TMD data, for various displacements. For a moderate $|\alpha|$, the measured parity is below the corresponding one for the vacuum and the Wigner function becomes slightly narrower, witnessing the presence of the quadrature squeezing. This effect is small, given the limited amount of squeezing available, but statistically significant and also happens with no mode overlap. We emphasize that, although this narrowing has been discussed already for pure states, as in Eq. (2), it also reveals squeezing for mixed states.

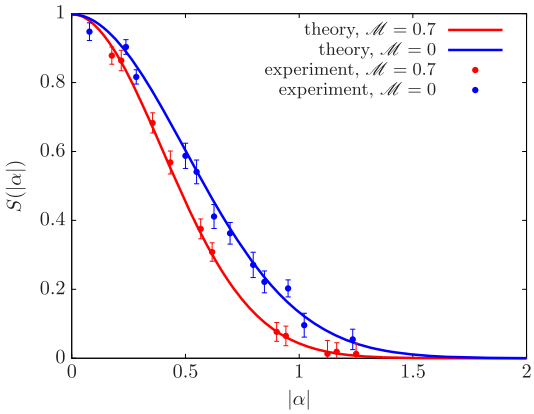

FIG. 3. Experimentally determined parities of a two-mode displaced PDC state with $r \approx 0.6$ as obtained with high overlap ($\mathcal{M} = 0.7$, red symbols) and no overlap ($\mathcal{M} = 0$, blue symbols) between the reference and signal modes. Theoretical predictions are also shown (the solid lines).

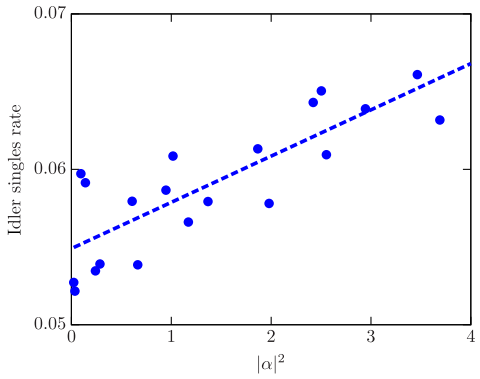

FIG. 4. Observed idler singles rate (the dots) for different signal displacements of a PDC state with $r \approx 0.6$. Best linear fit is also shown (the line).

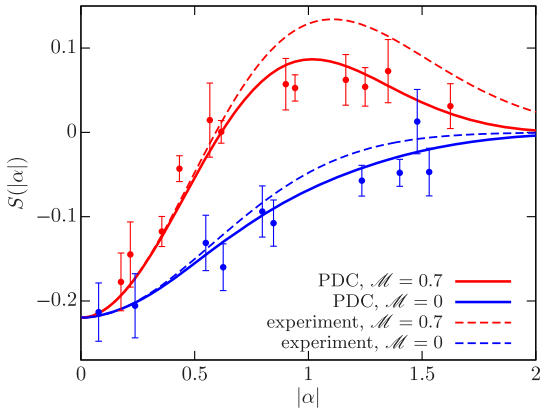

FIG. 5. Parities of heralded signal states measured with high overlap (the red symbols) and no overlap (the blue symbols) and $r \approx 0.6$. Solid (broken) lines show theory with afterpulses included (ignored). Notice that the afterpulses tend to decrease the measured parity of the displaced signal mode.

Next, we focus on heralding single-mode states by a single idler click. Ideally, such a heralding generates a single photon in the signal mode, a state characterized by a strongly negative Wigner function at the origin.

Heralding at telecom wavelengths is highly nontrivial due to the afterpulses in the idler counts. This effect can be ignored for weak undisplaced PDC states [31], but, for large displacements, afterpulses make up a significant fraction of the small number of genuine idler detections (more than 10% in our case). This is illustrated in Fig. 4, where the idler single-click detection rate is plotted as a function of the reference beam intensity $|\alpha|^2$. Without afterpulsing, the idler rates should stay constant, while we observe a linear increase of the idler detection rate with $|\alpha|^2$.

After a single idler detection, the postmeasurement state of the signal mode is $P_s = \mathrm{Tr}_i(\hat{E}\,\hat{P}\,\hat{E}^\dagger)/\mathrm{Tr}_{s,i}(\hat{E}\,\hat{P}\,\hat{E}^\dagger)$, where $\hat{E}^\dagger\hat{E} = \hat{\Pi}_{1s}$ is the operator describing the idler detection, and $\mathrm{Tr}_{s,i}$ indicates tracing over both the signal and idler modes. To deal with afterpulses, we construct the measurement operator as an incoherent superposition of signal and idler single detections, $\hat{E}^\dagger\hat{E} = [1 - x(\alpha)]\hat{\Pi}_{1i} + x(\alpha)\hat{\Pi}_{1s}$. The contribution of afterpulses for a given displacement is estimated from Fig. 4.

Afterpulses introduce a systematic negative bias into the reconstructed values of the signal parity. This is because heralding by an afterpulse increases the single-photon component of the signal state.

Experimental characterization of displaced heralded states measured with and without overlap between the signal and reference modes is summarized in Fig. 5. For high overlap, we expect the parity to trace the Wigner function of the heralded signal state, which can be approximated by a single-photon state. The negativity around the origin is apparent in the red curves (corrected for afterpulses). For no overlap, the measured parities remain negative for all displacements. The two cases can be discriminated, showing that the heralded states are very sensitive to previous interactions in the signal beam.

In Fig. 6 we show the reconstructed signal photon-number distributions P_n for three different displacements and $r \approx 0.6$. As the reference amplitude is increased, the vacuum components of the signal states are strongly suppressed. This could be expected. The heralded signal is approximately a single-photon state, $P_n^s \approx \delta_{1,n}$. With mode overlap switched on, this state is displaced by $|\alpha|$; with mode overlap switched off, the resulting photon-number distribution is simply a discrete convolution of the reference Poissonian distribution $P_n^r = |\alpha|^{2n}\exp(-|\alpha|^2)/n!$ and the signal single-photon distribution P_n^s. Obviously, the

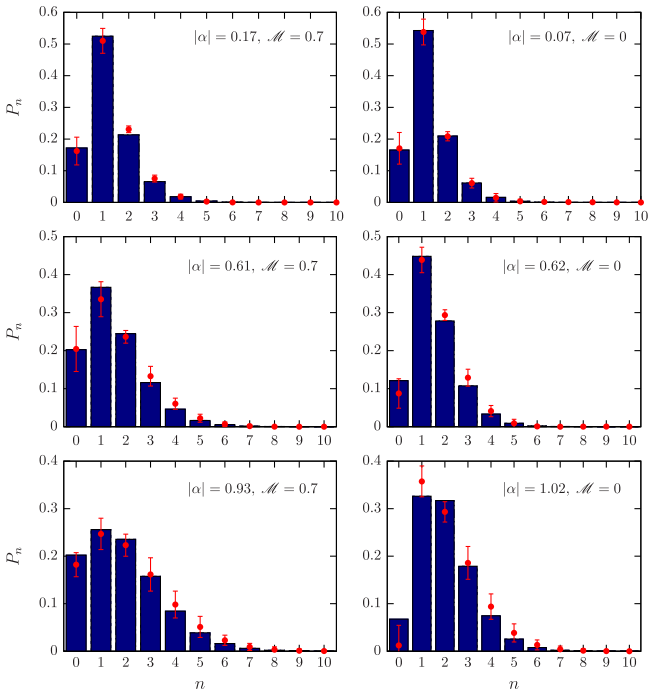

FIG. 6. Reconstructed signal photon-number distributions of heralded and displaced PDC states (the dots); $r \approx 0.6$. Theoretical models are also shown (the bars). Displacement increases from top to bottom. Left (right) panels correspond to strong (no) overlap between the reference and signal modes.

appearance of a Kronecker delta in such a convolution makes the reference Poissonian distribution displaced by one towards higher photon numbers, $P_n \approx P^r_{n-1}$ effectively erasing the vacuum component $P_0 \approx 0$.

It happens often that the full distribution P_{mn} is not required for a specific purpose. For example, only a few elements of P_{mn} or a linear function of P_{mn}, such as parity, might be enough. This is called partial tomography and finds applications in experiments with complex, highly dimensional systems, where a full tomography is impractical or even impossible. A nice feature of the pattern approach is that both full and partial tomography are done in much the same way. A demonstration of the technique is presented in the Supplemental Material [34].

In summary, we have directly probed the Wigner function of a nonclassical single-photon wave packet in a robust, loss-tolerant manner. Our TMD detector, with the tool of data pattern, can verify the nonclassicality and highlight the role of mode properties in the detection. This leads us to recognize the types of experimental imperfections and gives us valuable information about the degradation caused by each one.

G. H. and Ch. S. acknowledge the support from the EU Horizon 2020 research and innovation program (Qcumber, Grant No. 665148). J. R., Z. H., L. M., and B. S. are thankful for the financial assistance of the Grant Agency of the Czech Republic (Grant No. 15-03194S), the IGA Project of the Palacký University (Grant No. PRF 2016-005), and the Technology Agency of the Czech Republic (Grant No. TE01020229).

[1] *Quantum State Estimation*, edited by M. G. A. Paris and J. Řeháček, Lecture Notes in Physics Vol. 649 (Springer, Berlin, 2004).
[2] A. I. Lvovsky and M. G. Raymer, Continuous-variable optical quantum-state tomography, Rev. Mod. Phys. **81**, 299 (2009).
[3] A. Royer, Measurement of the Wigner Function, Phys. Rev. Lett. **55**, 2745 (1985).
[4] D. Leibfried, D. M. Meekhof, B. E. King, C. Monroe, W. M. Itano, and D. J. Wineland, Experimental Determination of the Motional Quantum State of a Trapped Atom, Phys. Rev. Lett. **77**, 4281 (1996).
[5] P. Bertet, A. Auffeves, P. Maioli, S. Osnaghi, T. Meunier, M. Brune, J. M. Raimond, and S. Haroche, Direct Measurement of the Wigner Function of a One-Photon Fock State in a Cavity, Phys. Rev. Lett. **89**, 200402 (2002).
[6] A. Kuzmich, I. A. Walmsley, and L. Mandel, Violation of Bell's Inequality by a Generalized Einstein-Podolsky-Rosen State Using Homodyne Detection, Phys. Rev. Lett. **85**, 1349 (2000).
[7] G. Donati, T. J. Bartley, X.-M. Jin, M.-D. Vidrighin, A. Datta, M. Barbieri, and I. A. Walmsley, Observing optical coherence across Fock layers with weak-field homodyne detectors, Nat. Commun. **5**, 5584 (2014).
[8] S. Wallentowitz and W. Vogel, Unbalanced homodyning for quantum state measurements, Phys. Rev. A **53**, 4528 (1996).
[9] K. Banaszek and K. Wódkiewicz, Direct Probing of Quantum Phase Space by Photon Counting, Phys. Rev. Lett. **76**, 4344 (1996).
[10] R. H. Hadfield, Single-photon detectors for optical quantum information applications, Nat. Photonics **3**, 696 (2009).
[11] J. L. O'Brien, A. Furusawa, and J. Vuckovic, Photonic quantum technologies, Nat. Photonics **3**, 687 (2009).
[12] G. S. Buller and R. J. Collins, Single-photon generation and detection, Meas. Sci. Technol. **21**, 012002 (2010).
[13] C. M. Natarajan, M. G. Tanner, and R. H. Hadfield, Superconducting nanowire single-photon detectors: Physics and applications, Supercond. Sci. Technol. **25**, 063001 (2012).
[14] B. Calkins, P. L. Mennea, A. E. Lita, B. J. Metcalf, W. S. Kolthammer, A. Lamas-Linares, J. B. Spring, P. C. Humphreys, R. P. Mirin, J. C. Gates, P. G. R. Smith, I. A. Walmsley, T. Gerrits, and S. W. Nam, High quantum-efficiency photon-number-resolving detector for photonic on-chip information processing, Opt. Express **21**, 22657 (2013).
[15] J. Wenger, J. Fiurášek, R. Tualle-Brouri, N. J. Cerf, and P. Grangier, Pulsed squeezed vacuum measurements without homodyning, Phys. Rev. A **70**, 053812 (2004).
[16] D. Achilles, Ch. Silberhorn, C. Śliwa, K. Banaszek, and I. A. Walmsley, Fiber-assisted detection with photon number resolution, Opt. Lett. **28**, 2387 (2003).
[17] J. Řeháček, Z. Hradil, O. Haderka, J. Peřina, and M. Hamar, Multiple-photon resolving fiber-loop detector, Phys. Rev. A **67**, 061801 (2003).
[18] M. J. Fitch, B. C. Jacobs, T. B. Pittman, and J. D. Franson, Photon-number resolution using time-multiplexed single-photon detectors, Phys. Rev. A **68**, 043814 (2003).
[19] D. Achilles, Ch. Silberhorn, and I. A. Walmsley, Direct, Loss-Tolerant Characterization of Nonclassical Photon Statistics, Phys. Rev. Lett. **97**, 043602 (2006).
[20] K. Laiho, K. N. Cassemiro, D. Gross, and Ch. Silberhorn, Probing the Negative Wigner Function of a Pulsed Single Photon Point by Point, Phys. Rev. Lett. **105**, 253603 (2010).
[21] A. Luis and L. L. Sánchez-Soto, Complete Characterization of Arbitrary Quantum Measurement Processes, Phys. Rev. Lett. **83**, 3573 (1999).
[22] J. Fiurášek, Maximum-likelihood estimation of quantum measurement, Phys. Rev. A **64**, 024102 (2001).
[23] G. M. D'Ariano, L. Maccone, and P. Lo Presti, Quantum Calibration of Measurement Instrumentation, Phys. Rev. Lett. **93**, 250407 (2004).
[24] J. S. Lundeen, A. Feito, H. Coldenstrodt-Ronge, K. L. Pregnell, Ch. Silberhorn, T. C. Ralph, J. Eisert, M. B. Plenio, and I. A. Walmsley, Tomography of quantum detectors, Nat. Phys. **5**, 27 (2009).
[25] T. Amri, J. Laurat, and C. Fabre, Characterizing Quantum Properties of a Measurement Apparatus: Insights from the Retrodictive Approach, Phys. Rev. Lett. **106**, 020502 (2011).
[26] L. Zhang, A. Datta, H. B. Coldenstrodt-Ronge, X.-M. Jin, J. Eisert, M. B. Plenio, and I. A. Walmsley, Recursive quantum detector tomography, New J. Phys. **14**, 115005 (2012).
[27] G. Brida, L. Ciavarella, I. P. Degiovanni, M. Genovese, L. Lolli, M. G. Mingolla, F. Piacentini, M. Rajteri, E. Taralli, and M. G. A. Paris, Quantum characterization of superconducting photon counters, New J. Phys. **14**, 085001 (2012).

[28] J. Řeháček, D. Mogilevtsev, and Z. Hradil, Operational Tomography: Fitting of Data Patterns, Phys. Rev. Lett. **105**, 010402 (2010).

[29] D. Mogilevtsev, A. Ignatenko, A. Maloshtan, B. Stoklasa, J. Rehacek, and Z. Hradil, Data pattern tomography: Reconstruction with an unknown apparatus, New J. Phys. **15**, 025038 (2013).

[30] M. Cooper, M. Karpinski, and B. J. Smith, Local mapping of detector response for reliable quantum state estimation, Nat. Commun. **5**, 4332 (2014).

[31] G. Harder, C. Silberhorn, J. Rehacek, Z. Hradil, L. Motka, B. Stoklasa, and L. L. Sánchez-Soto, Time-multiplexed measurements of nonclassical light at telecom wavelengths, Phys. Rev. A **90**, 042105 (2014).

[32] M. Altorio, M. G. Genoni, F. Somma, and M. Barbieri, Metrology with Unknown Detectors, Phys. Rev. Lett. **116**, 100802 (2016).

[33] G. Harder, V. Ansari, B. Brecht, T. Dirmeier, C. Marquardt, and C. Silberhorn, An optimized photon pair source for quantum circuits, Opt. Express **21**, 13975 (2013).

[34] See Supplemental Material at http://link.aps.org/supplemental/10.1103/PhysRevLett.116.133601 for a brief description of the fitting of data pattern and the related partial tomography.